Radiometric Calibration from Noise Distributions

Yasuyuki Matsushita Stephen Lin
Microsoft Research Asia
Beijing, P.R. China, 100080
Email: {yasumat,stevelin}@microsoft.com

Abstract

A method is proposed for estimating radiometric response functions from noise observations. From the statistical properties of noise sources, the noise distribution for each scene radiance value is shown to be symmetric for a radiometrically calibrated camera. However, due to the non-linearity of camera response functions, the observed noise distributions become skewed in an uncalibrated camera. In this paper, we capitalize on these asymmetric profiles of measured noise distributions to estimate radiometric response functions. Unlike prior approaches, the proposed method is not sensitive to noise level, and is therefore particularly useful when the noise level is high. Also, the proposed method does not require registered input images taken with different exposures; only statistical noise distributions at multiple intensity levels are used. Real-world experiments demonstrate the effectiveness of the proposed approach in comparison to standard calibration techniques.

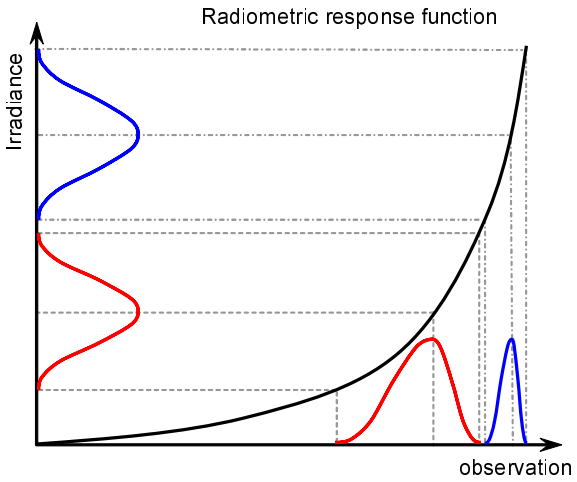

Figure 1. The symmetric profile of a noise distribution in the image irradiance domain becomes skewed by the non-linearity of the radiometric response function. The profile of the measured noise distribution becomes asymmetric accordingly.

1. Introduction

Many computer vision algorithms rely on the assumption that image intensities are linearly related to the image irradiance recorded at the camera sensor. Since most cameras non-linearly alter irradiance values for purposes such as dynamic range compression, this assumption generally does not hold. It is therefore important to calibrate the response function of a camera, so that the non-linear mapping can be inverted and subsequent algorithms can assume linearity of intensity observations.

As stated by the late Rolf Landauer, a founder of mesoscopic physics, noise is a signal [10]. Fluctuations of a measurement in time, or the distribution of fluctuations, can offer information that cannot be found in the time-averaged value. This observation is exploited in noise thermometry, an established technique for measuring temperature in high-pressure environments based on the level of electric noise. Likewise, image noise can provide valuable information about the imaging process, and we show in this paper that the noise distribution in observed images reveals the shape of the radiometric response function. Because of the symmetrically random nature of noise sources in the imaging process, asymmetry of noise distributions in a measured image is the result of a non-linear transformation that occurs in the camera due to the radiometric response function. Based on this observation, our method estimates the inverse response function as the function that maps the asymmetric distribution of noise in the observation domain to a symmetric distribution in the irradiance domain. This idea is illustrated in Figure 1.

The primary contributions of our work are twofold. First, it introduces the use of image noise as a signal for estimating radiometric response functions. Noise has widely been considered a nuisance in computer vision, but here we derive an important benefit from noise observations. Second, the proposed radiometric calibration method is effective at high noise levels, which can substantially degrade previous radiometric calibration techniques. Our method examines only the symmetry of noise distributions, which is not affected by noise level. Since noise is inevitable in real im-

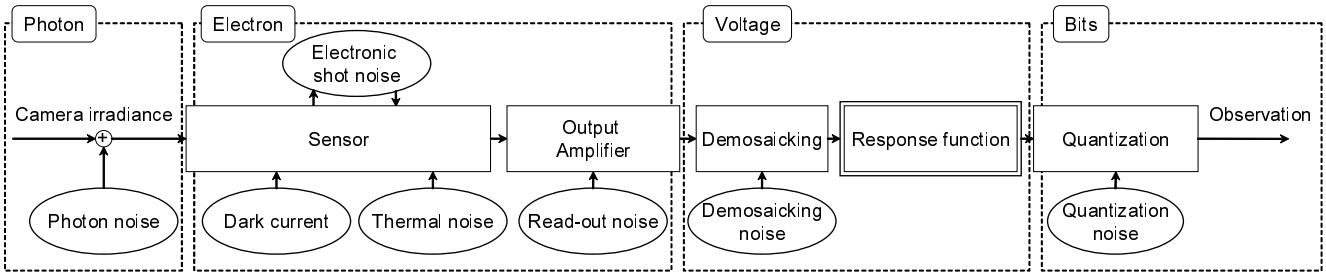

Figure 2. Imaging process and noise sources of digital cameras.

ages, the proposed method has wide applicability.

Since the noise characteristics of a camera typically vary with respect to irradiance value, our technique takes as input the noise distributions for different image irradiances. This data can be collected by capturing multiple images of a fixed scene, or by combining intensity data from uniform scene regions in a single image, as done in [13]. With the proposed approach, calibration results that match those of standard techniques can be computed from less data, by capitalizing on a new source of calibration information.

1.1. Background

Radiometric calibration aims to estimate the response function f of a camera. The radiometric response function f maps irradiance I that is captured at the sensor to the image intensity M that is read from the camera:

$$M = f(I). \tag{1}$$

For vision algorithms that require irradiance values I rather than measured intensity M as input, the inverse response function $g = f^{-1}$ needs to be determined so that measured intensities can be made linear with respect to irradiances. Since response functions f are monotonic, they are invertible. As in most previous radiometric calibration methods, we assume in this work that the sensor response does not change over the image.

1.2. Prior work

Several methods have been proposed to estimate the camera response function. Most of them require as input an image sequence taken with varying exposures from a fixed camera. With known ratios among exposure levels, Mann and Picard [15] compute a parametric response function in the form of a gamma curve, and Debevec and Malik [4] obtain a nonparametric response function using a smoothness constraint. With only approximate knowledge of relative exposure levels, Mitsunaga and Nayar [16] iteratively solve for a response function based on the assumption that it has a polynomial form. Other iterative estimation methods include that of Tsin *et al*. [22], which estimates nonparametric responses using a statistical model of the CCD imaging process, and of Pal *et al*. [20], which utilizes probabilistic imaging models and prior models of response functions to compute response functions that can differ from image to image.

A few prior methods allow some camera movement or scene motion, but still require changes in exposure level. Mann [14] presents a method for response function estimation from image sequences taken by a rotating and zooming camera. Kim and Pollefeys [9] compute point correspondences to allow free movement of the camera and some motion in the scene. Grossberg and Nayar [6] avoid reliance on spatial correspondences by relating histogrammed intensity values between two images of different exposure.

In many applications such as those for web cameras, multiple images at different exposures cannot be obtained for radiometric calibration. Some previous techniques have been presented without the need to make adjustments in camera exposure settings. Nayar and Mitsunaga [17] place an optical filter with spatially varying transmittance on the imaging array, which effectively leads to different exposures for neighboring pixels. The response function can then be computed from neighboring pixels that have different exposures but equal scene brightness. Farid [5] proposes a gamma correction technique based on the frequency-domain correlations that it introduces to an image. This approach requires assumptions on the statistics of scene radiance, and the radiometric responses of many cameras differ significantly from a gamma function.

A more general approach based on edge information in single-image input was proposed by Lin *et al*. for color images [11] and for grayscale images [12]. The former obtains information about the radiometric response function from color distributions of local edge regions. Due to blending of distinct region colors, irradiance colors from edge regions should form linear distributions in color space. But because of nonlinear radiometric response functions, measured edge colors actually compose nonlinear distributions that are directly related to the response function. With a prior model of response functions compiled by Grossberg and Nayar [7], the inverse radiometric response is computed as the function that maps the nonlinear distributions of measured edge colors into linear distributions. For grayscale images, a 1D

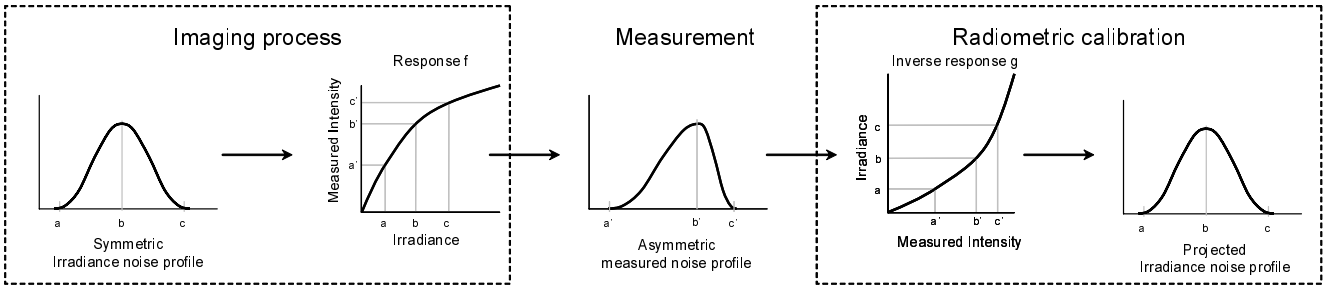

Figure 3. Illustration of our method. Symmetric noise profiles are skewed by the radiometric response function in the imaging process. Radiometric calibration is performed by estimating a function that transforms the skewed noise distributions into symmetric forms.

analogue of the 3D color method is presented in [12].

Our work may be considered as complementary to the methods based on edge information. Since the edge-based methods rely on statistical distributions from possibly sparse data, they may be susceptible to high levels of image noise. In contrast, our technique utilizes noise as an information source. Our method is also able to use non-edge regions in an image for radiometric calibration. In principle, a single-image technique could be developed that combines the edge processing of [11] together with our proposed approach applied to uniform regions in the image.

2. Transformation of noise distributions

Figure 2 outlines the imaging process and sources of noise. Our method is built upon the assumption that the noise distributions from the various noise sources are statistically symmetric. In this section, we first review the properties of the different types of noise in the imaging pipeline, and confirm the validity of this assumption. Then we describe the transformation of these symmetric noise distributions by nonlinear camera response functions into asymmetric distributions in measured images.

2.1. Symmetry of imaging noise

In the imaging process, radiance from the scene is first focused by the lens onto the sensor. This scene radiance fluctuates over time due to the discrete nature of photons. These temporal fluctuations are called photon noise, or photon shot noise. Photon noise obeys the Poisson law [3, 1], and a Poisson distribution is well-approximated by a Gaussian distribution when the number of arrivals is large [21]. Since the number of photon arrivals at an sensor element can be considered large under ordinary imaging conditions, the distribution of photon noise can reasonably be approximated as Gaussian. Photon noise is therefore symmetric.

The incoming rays are then captured by the imaging sensor and converted to an electrical signal. In the process of conversion, the signal is contaminated by dark current, shot noise, and thermal noise. Dark current adds a constant offset to the signal with zero-mean fluctuations. This fluctuation is called dark current noise, or thermal noise. Dark current noise arises from thermally generated charges in the sensor. Due to manufacturing variances, some pixels in the sensor have greater dark current than others. These pixels are referred to as hot pixels, and are a source of fixed pattern noise. Since dark current noise occurs in the form of discrete electrons, the noise process obeys the Poisson law. Electronic shot noise, which is different from photon shot noise, occurs in the electronic circuitry due to random fluctuations of current in an electrical conductor. These fluctuations similarly arise from the fact that current is carried by discrete electrons. These sources of noise at the sensor all obey the Poisson process. Since the number of electrons involved per pixel is large, their noise distributions are also well-approximated by a Gaussian.

An output amplifier sequentially transforms the electrons from each pixel into a voltage. The amplifier adds read-out noise, whose distribution is zero-mean and independent of the number of captured electrons. Read-out noise can be treated as having a symmetric distribution since it results from the random effects of coupled sources: that counting of electrons is not a perfectly repeatable process, and that spurious electrons exist within the amplifier.

In the case of color cameras, a demosaicking process converts the raw sensor signal into a three-channel color image by interpolating the red, green, and blue pixels in the imaging array. This process can affect the noise distributions for interpolated pixel values, since they are being estimated from other noisy signals. Since interpolation is computed among measurements with symmetric noise distributions, we regard the noise distributions of demosaicked color values also to be statistically symmetric.

At this point, the demosaicked irradiance value is then transformed to the measured intensity by the camera's radiometric response function f. In this process, the symmetric profiles of the noise distributions becomes distorted by the non-linearity of the camera response function, as further described in Section 2.2.

Finally the signal is quantized, and quantization noise is introduced. Since quantization noise results from the rounding of signal amplitudes to discrete levels, it can be consid-

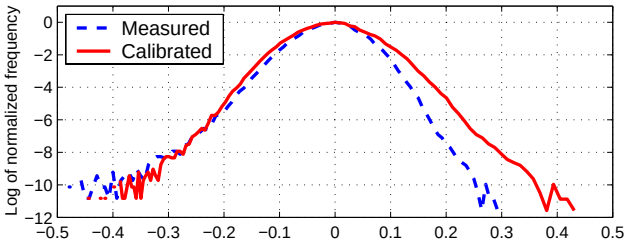

Figure 4. A noise profile measured using a Canon EOS 20D (ISO 1600), and the corresponding noise profile after calibration with the ground truth response curve. The noise profiles are scaled horizontally for better visualization.

ered as a zero mean random variable with a uniform probability distribution [19].

2.2. Asymmetry of measured noise

As reviewed above, all noise sources in a digital camera can be considered statistically symmetric. For a camera with a linear response function, its observed noise distributions should therefore be symmetric. On the other hand, non-linearity of the radiometric response function will lead to asymmetry in the observed noise distributions, as illustrated in Figure 3. For typical response functions, the non-linear mapping results in greater condensation of the distribution towards higher intensities and broadening towards lower intensities. This leads to measured noise distributions that are negatively skewed.

The correct inverse response function g should transform the asymmetric profile of the measured noise distribution to a symmetric profile as illustrated in Figure 3 (right). In Figure 4, we show a real-world example of how a measured asymmetric noise profile is projected using the ground truth response function into a symmetric distribution in the irradiance domain. Our work aims to find such a function for radiometric calibration.

3. Calibration algorithm

In presenting our calibration algorithm, we first describe how we evaluate the degree of symmetry of a noise profile. Based on this symmetry measure, we then derive an energy function that estimates the inverse response function g that best transforms measured noise profiles to symmetric forms. For cases where the available noise data is insufficient to avoid solution ambiguities, we utilize a prior model of inverse response functions to regulate the solution.

3.1. Degree of symmetry

There exist various possible approaches to measuring the symmetry of a statistical distribution. Since the mean, median and mode are all the same in a symmetric distribution,

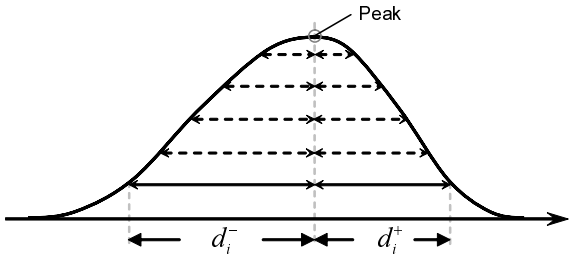

Figure 5. Evaluation of the degree of distribution symmetry.

one basic symmetry metric is Pearson's skewness coefficients $S_1 = 3(\bar{x} - \tilde{x})/\sigma$ and $S_2 = 3(\bar{x} - \check{x})/\sigma$, with distribution mean $\bar{x}$, mode $\tilde{x}$, median $\check{x}$, and standard deviation σ [8]. Values of these two coefficients that are closer to zero indicate greater distributional symmetry.

In this work, we evaluate symmetry in a manner that is similar to the Bowley skewness [8], which computes distances among interquartile ranges to effectively obtain a measure of distribution balance around its median. In our symmetry metric, we compute the distance from the distribution mode to the profile of the distribution at multiple different heights as shown in Figure 5. At each i-th height in the distribution q, the distance to the profile on the left $d_{q,i}^-$ and on the right $d_{q,i}^+$ are respectively computed. The degree of symmetry of the distribution q is then evaluated as

$$S(q) = -\frac{1}{n}\sum_{i=1}^{n}\left(\frac{d_{q,i}^- - d_{q,i}^+}{d_{q,i}^- + d_{q,i}^+}\right)^2, \qquad (2)$$

where n is the number of heights to be evaluated. A larger value of n yields a more accurate result at the expense of greater computation time, which is proportional to n. The denominator normalizes each term by the distribution width at the given height. Larger values of S indicate greater symmetry.

While the inverse of any skewness metric could in principle be used in place of Equation (2), we utilize this measure because of its effectiveness in optimization. In contrast, we have empirically found the Bowley skewness and Pearson's skewness coefficients to be less sensitive to the slight changes in distribution structure that occur in an iterative optimization procedure.

3.2. Solution method

With this symmetry measure, our method computes the inverse response function g from the set of collected noise profiles Ω by maximizing the following energy function:

$$E(g;\Omega) = \frac{1}{|\Omega|}\sum_{q\in\Omega} S(g;q) = \frac{1}{|\Omega|}\sum_{q\in\Omega} S(g(q)), \qquad (3)$$

where $|\Omega|$ represents the number of noise distributions in the set Ω. This function evaluates the degree of symmetry

of noise profiles that are projected to the irradiance domain by the inverse response function g.

While $\text{argmax}_g E(g)$ gives the optimal estimate of the inverse response function g, it is computationally difficult to solve for a non-parametric inverse response function, because of the large number of intensity levels (e.g., 256 for 8-bit images). To facilitate optimization, we utilize a parametric model based on Grossberg and Nayar's principal components analysis (PCA) on the DoRF database of real-world response functions [7]. The response functions in the DoRF database are first inverted so that principal components of inverse response functions can be computed. With these principal components, an inverse response function g can be represented as

$$g = g_0 + \mathbf{H}c, \tag{4}$$

where g_0 is the mean inverse response, $\mathbf{H}$ is the matrix whose columns are composed of the first N eigenvectors, and c is an N-dimensional vector of PCA coefficients. In this work we set $N = 5$ as done in [7, 12]. With this representation of inverse response functions, the problem is transformed into estimating the N coefficients of c:

$$\hat{c} = \underset{c}{\text{argmax}}\, E(g; g = g_0 + \mathbf{H}c). \tag{5}$$

3.3. Solution using prior model

In cases where the projected noise profiles $g(\forall q \in \Omega)$ do not cover the entire range of irradiance values, there may exist multiple solutions that result in symmetry of noise distributions. To avoid this ambiguity, additional constraints on the inverse response function, such as smoothness and monotonicity, could be used. In this paper, we use prior data from the DoRF database to regulate the solution as done in [12].

Using the eigenvectors of Equation (4), we compute the PCA coefficients of each inverse response function in DoRF. We then construct a prior model on inverse responses by fitting a multivariate Gaussian mixture model to this set of PCA coefficients:

$$p(g) = \sum_{i=1}^{K} \alpha_i \mathcal{N}(g; \mu_i, \Sigma_i), \tag{6}$$

where $\mathcal{N}$ represents a normal distribution with mean μ_i and covariance matrix Σ_i. We empirically set $K = 5$, and the mixture model is obtained using the cross-entropy method [2].

We also model the likelihood of the degree of symmetry as

$$p(\Omega|g) = \frac{1}{Z} \exp(-\lambda E(g; \Omega)), \tag{7}$$

where Z is the normalization factor, and λ is a regularization coefficient, which is empirically set to 10^4.

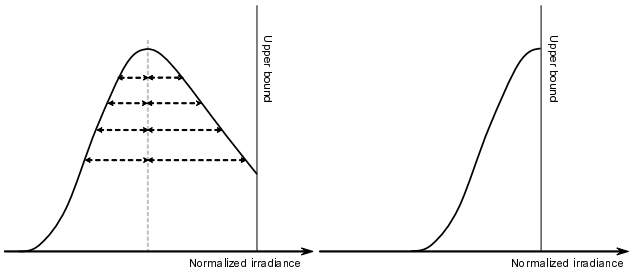

(a) (b)

Figure 6. Processing of incomplete noise distributions. (a) Upper portion of noise profile is used for evaluating the degree of symmetry. (b) Noise profile is discarded due to insufficient symmetry data.

The optimal coefficients $\hat{c}$ that define the inverse response function g are solved in the following MAP problem:

$$\hat{c} = \underset{c}{\text{argmax}}\, p(g(c)|\Omega) = \underset{c}{\text{argmax}}\, p(\Omega|g(c))p(g(c)). \tag{8}$$

Inserting Equations (6) and (7) into the logarithmic form of Equation (8), we obtain

$$\hat{c} = \underset{c}{\text{argmin}}\, \lambda E(g(c); \Omega) - \log p(g(c)). \tag{9}$$

The optimized coefficients $\hat{c}$ yield our estimate of the inverse response function as $\hat{g} = g_0 + \mathbf{H}\hat{c}$.

4. Experiments

To evaluate our method, we performed experiments on various real-world cameras and scenes. In our implementation, optimization is performed using the Nelder-Mead simplex method [18] with multiple initial values. The degree of symmetry in Equation (2) is evaluated with $n = 20$ for all examples in this paper. The evaluation is performed in the irradiance domain as described in Equation (3). At the lower and upper bounds of the intensity range where a complete noise profile cannot be observed, we use only the available partial profile in computing the degree of symmetry, as illustrated in Figure 6.

In our experiments, we first examine cases where noise distributions are recovered over the entire range of intensity levels. We then consider the case of incomplete data, which utilizes the prior model of inverse response functions to determine a solution.

Results with complete data In this experiment, we efficiently measure noise distributions at different intensity levels by capturing a static scene with a fixed video camera. With this setup, the intensity fluctuations at a pixel over time are caused only by noise. By combining the intensity observations of a pixel into a histogram, noise distributions

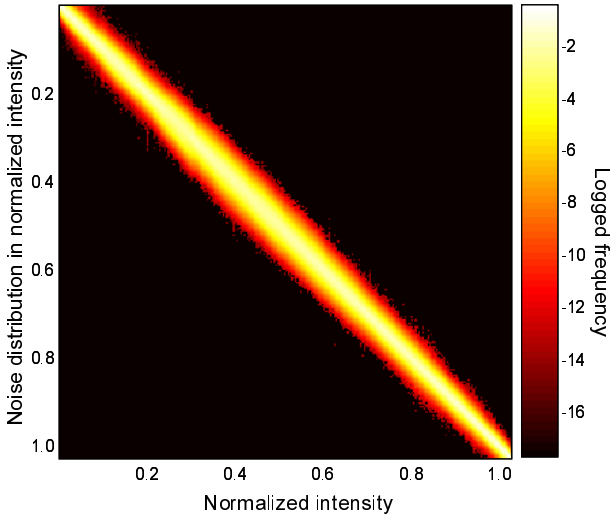

Figure 7. Measured noise distributions (Sony DSR-PD190P). The logarithm of normalized frequency values are used for visualization purposes. Each vertical slice represents a noise distribution at the corresponding intensity level.

Camera	RMSE	Disparity
JVC GR-D230AH	0.0224	0.0495
Sony DCR-TRV9E	0.0247	0.0522
Sony DSR-PD190P	0.0332	0.0673
PointGrey DragonFly	0.0265	0.0478

Table 1. RMSE and disparity of estimated inverse response functions in terms of normalized irradiance.

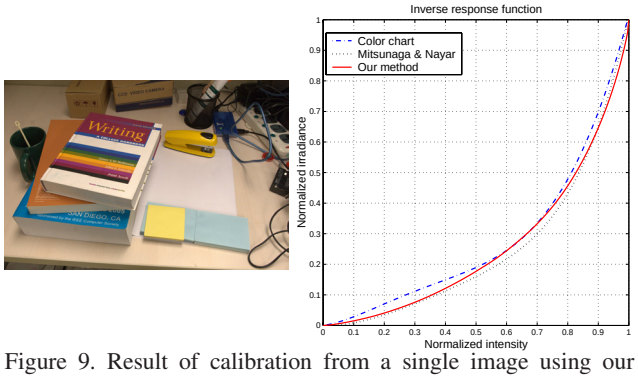

Figure 9. Result of calibration from a single image using our method. The scene is photographed at an ISO 800 gain level.

are directly measured for each pixel. Furthermore, these collected noise distributions from the image set are merged together according to intensity level for greater statistical stability. The mode of each measured noise distribution is taken as its true intensity.

We used four different video cameras for experiments: JVC GR-D230AH, Sony DCR-TRV9E, Sony DSR-PD190P, and PointGrey DragonFly. Each input dataset is collected by capturing a static scene for 100 frames (about 3 secs at 30 fps). In this experiment, we ensure that noise distributions are acquired over the full range of intensity levels. This can often be achieved simply by capturing two image sequences of a scene at different exposure levels, e.g., one bright scene and one dark scene, and then merging them together to form a single dataset. Figure 7 shows a measured noise distribution for the Sony DSR-PD190P camera. Each column of the chart represents the noise distribution of the corresponding intensity level.

Representative results of the proposed method are shown in Figure 8. In the figure, comparisons of our estimated inverse response curves to those of standard radiometric calibration methods are shown in the left column. The center column displays the measured noise profiles and the resulting symmetric noise profiles after applying the estimated inverse response functions. For better visualization, the noise profiles are displayed at every ten intensity levels starting from intensity level 5. In actual computation, the noise profiles for all intensity levels are used to estimate the inverse response functions.

For a quantitative comparison of our method to standard techniques, we evaluated the RMSE (root-mean-squared error) in terms of normalized irradiance and disparity, which represents the average value among the dataset of the maximum difference between our function and the comparison curve. In computing disparity, four sequences for each camera are used. The result is summarized in Table 1. For the Sony DSR-PD190P and PointGrey DragonFly cameras, the comparison curve is generated by averaging the curves obtained by the method in [16] and by fitting to Macbeth color checker measurements, which were interpolated using a fifth-degree polynomial. For the JVC GR-D230AH and Sony DCR-TRV9E cameras, the inverse response function obtained using the Macbeth color checker is used as the comparison curve. The low RMSE and disparity values demonstrate an agreement between our calibration method and the standard techniques, which utilize additional data such as multiple exposure settings or known relative scene colors.

Results with incomplete data When the observed noise distributions do not span the entire range of intensity levels, we use the prior model on inverse response functions to constrain the solution as described in Section 3.3. We conduct this experiment using a single input image that does not include a full range of intensities. For simplicity in validating our method, we photographed a scene composed of relatively flat, uniform surfaces, and then manually selected image regions from which to obtain noise distributions. A more sophisticated algorithm such as in [13] could alternatively be used to automate this process.

Figure 9 shows a result from a single input image using the prior. The RMSE and disparity are 0.0337 and 0.096 re-

spectively using five datasets, where the ground truth curve is computed as the mean curve between those obtained using a Macbeth color chart and the method of Mitsunaga & Nayar [16]. The relatively large disparity value likely results from the limited number of observations per noise distribution, which degrades the accuracy of the distributions in a statistical sense. Our solution nevertheless exhibits a close match to the ground truth curve.

5. Discussion

Symmetry assumption Our method is based on the assumption of symmetric noise distributions from the various sources. As we reviewed in Section 2, the assumption is valid under typical conditions where the numbers of photons and electrons in the sensor are sufficiently large. However, this assumption breaks down in low-light conditions, where photon and electron counts become small. In low-light conditions, photon noise and electronic shot noise distributions deviate from Gaussian approximation, and hence the symmetry assumption breaks down. The proposed method is therefore not intended for low-light images/videos.

Statistical validity of noise distributions For the measured noise distributions to be statistically valid, a sufficiently large number of samples per intensity level needs to be collected. One indicator of data sufficiency is the smoothness of the measured noise profiles. Since noise distributions are expected to be smooth, a coarse profile suggests inadequate sampling, and more image data is needed for greater reliability in radiometric calibration.

Future work In this work, we presented a radiometric calibration technique that takes advantage of the image noise that normally degrades computer vision algorithms. Its tolerance of high noise levels and effectiveness without multiple exposures are its primary benefits over previous algorithms. Because of these particular advantages, an interesting direction for future work is in employing our technique in a conjunctive manner with other radiometric calibration methods, to reduce sensitivity to noise and to resolve solution ambiguity in cases there would otherwise be little calibration data.

References

[1] F. Alter, Y. Matsushita, and X. Tang. An intensity similarity measure in low-light conditions. In *Proc. of European Conf. on Comp. Vis. (ECCV)*, pp. 267–280, 2006. 3

[2] Z. Botev and D. Kroese. Global likelihood optimization via the cross-entropy method with an application to mixture models. In *Proc. of the 36th Conf. on Winter simulation*, pp. 529–535, 2004. 5

[3] N. Campbell. Discontinuities in light emission. *Proc. Cambridge Phil. Soc.*, 15:310–328, 1909. 3

[4] P. E. Debevec and J. Malik. Recovering high dynamic range radiance maps from photographs. In *Proc. of ACM SIGGRAPH*, pp. 369–378, 1997. 2

[5] H. Farid. Blind inverse gamma correction. *IEEE Transactions on Image Processing*, 10(10):1428–1433, 2001. 2

[6] M. D. Grossberg and S. K. Nayar. Determining the camera response from images: What is knowable? *IEEE Trans. on Pattern Analysis and Machine Intelligence*, 25(11):1455–1467, 2003. 2

[7] M. D. Grossberg and S. K. Nayar. What is the space of camera response functions? In *Proc. of Comp. Vis. and Pattern Rec. (CVPR)*, vol. 2, pp. 602–609, 2003. 2, 5

[8] J. Kenney and E. Keeping. *Mathematics of Statistics, Pt. 1, 3rd ed.* Van Nostrand, 1962. 4

[9] S. Kim and M. Pollefeys. Radiometric alignment of image sequences. In *Proc. of Comp. Vis. and Pattern Rec. (CVPR)*, vol. 1, pp. 645–651, 2004. 2

[10] R. Landauer. Condensed-matter physics: The noise is the signal. *Nature*, 392:658–659, 1998. 1

[11] S. Lin, J. Gu, S. Yamazaki, and H. Y. Shum. Radiometric calibration from a single image. In *Proc. of Comp. Vis. and Pattern Rec. (CVPR)*, vol. 2, pp. 938–945, 2004. 2, 3

[12] S. Lin and L. Zhang. Determining the radiometric response function from a single grayscale image. In *Proc. of Comp. Vis. and Patt. Rec. (CVPR)*, vol. 2, pp. 66–73, 2005. 2, 3, 5

[13] C. Liu, W. T. Freeman, R. Szeliski, and S. B. Kang. Noise estimation from a single image. In *Proc. of Comp. Vis. and Pattern Rec. (CVPR)*, pp. 901–908, 2006. 2, 6

[14] S. Mann. Comparametric imaging: Estimating both the unknown response and the unknown set of exposures in a plurality of differently exposed images. In *Proc. of Comp. Vis. and Pattern Rec. (CVPR)*, vol. 1, pp. 842–849, 2001. 2

[15] S. Mann and R. Picard. Being 'undigital' with digital cameras: extending dynamic range by combining differently exposed pictures. In *Proc. of IS & T, 48th annual conference*, pp. 422–428, 1995. 2

[16] T. Mitsunaga and S. K. Nayar. Radiometric self-calibration. In *Proc. of Comp. Vis. and Pattern Rec. (CVPR)*, vol. 2, pp. 374–380, 1999. 2, 6, 7

[17] S. K. Nayar and T. Mitsunaga. High dynamic range imaging: Spatially varying pixel exposures. In *Proc. of Comp. Vis. and Pattern Rec. (CVPR)*, vol. I, pp. 472–479, 2000. 2

[18] J. A. Nelder and R. Mead. A simplex method for function minimization. *Computer Journal*, 7:308–313, 1965. 5

[19] A. Oppenheim and R. Schafer. *Digital Signal Processing*. Prentice Hall, 1975. 4

[20] C. Pal, R. Szeliski, M. Uyttendale, and N. Jojic. Probability models for high dynamic range imaging. In *Proc. of Comp. Vis. and Pattern Rec. (CVPR)*, vol. 2, pp. 173–180, 2004. 2

[21] S. Rice. Mathematical analysis of random noise. *Bell Syst. Tech. J.*, 23:282–332, 1944. 3

[22] Y. Tsin, V. Ramesh, and T. Kanade. Statistical calibration of ccd imaging process. In *Proc. of Int'l Conf. on Comp. Vis. (ICCV)*, vol. 1, pp. 480–487, 2001. 2

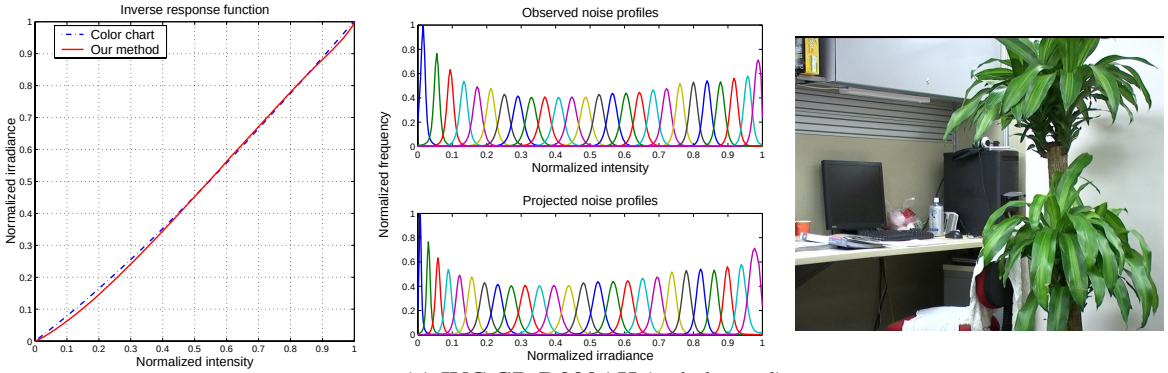

(a) JVC GR-D230AH (red channel)

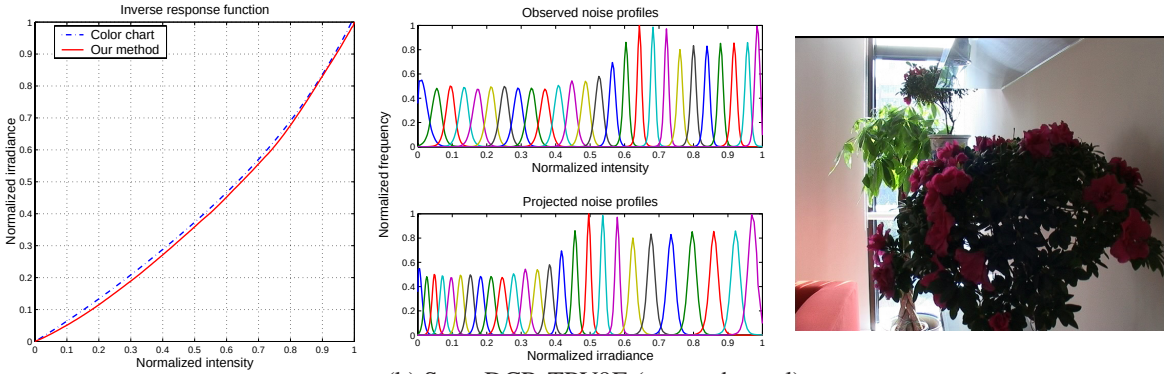

(b) Sony DCR-TRV9E (green channel)

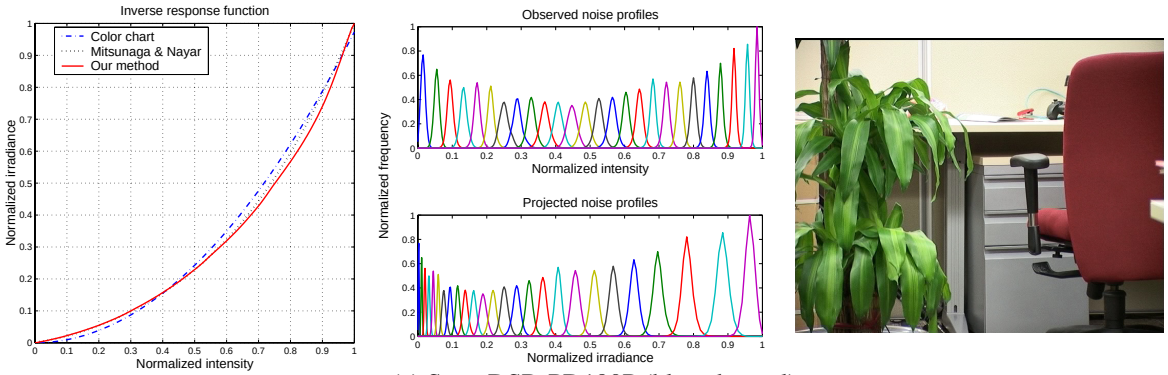

(c) Sony DSR-PD190P (blue channel)

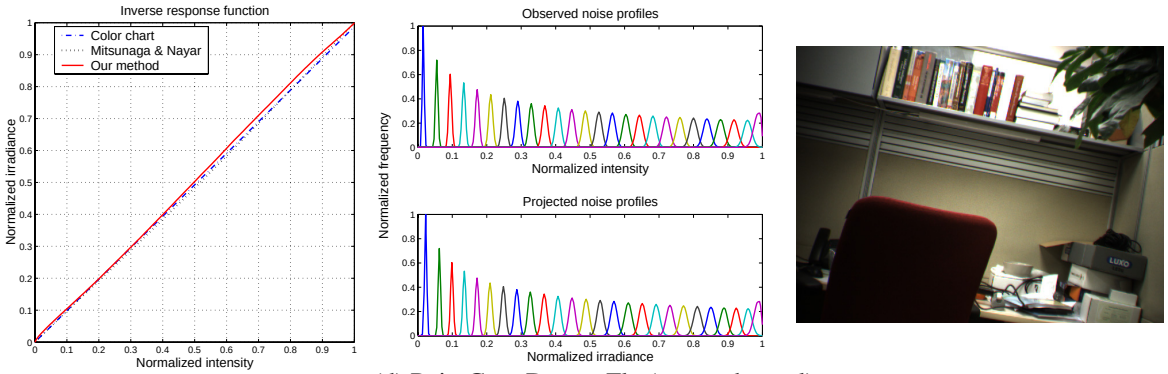

(d) PointGrey DragonFly (green channel)

Figure 8. Results of our radiometric calibration method. Left column: comparison of inverse response functions. Middle column: observed noise profiles and transformed noise profiles. Right column: an image from the corresponding test image sequence. Noise profiles are displayed at every ten intensity levels for visualization purposes. From top to bottom, the results of different cameras are shown: (a) JVC GR-D230AH, (b) Sony DCR-TRV9E, (c) Sony DSR-PD190P, and (d) PointGrey DragonFly.